Molecular Vision 2024; 30:260-267 <http://www.molvis.org/molvis/v30/260>
Received 1 May 2023 | Accepted 20 June 2024 | Published 26 June 2024

A potential novel role of the R36P mutation in CRYGD in congenial cataract

Chen Tan,[1] Xueting Yu,[1] Junyi Chen,[1] Xinghuai Sun,[1,2,3] Li Wang[1]

[1]Department of Ophthalmology and Visual Science, Eye and ENT Hospital, Shanghai Medical College, Fudan University, Shanghai, China; [2]NHC Key Laboratory of Myopia, Chinese Academy of Medical Sciences, Shanghai Key Laboratory of Visual Impairment and Restoration (Fudan University), Shanghai, China; [3]State Key Laboratory of Medical Neurobiology and MOE Frontiers Center for Brain Science, Institutes of Brain Science, Fudan University, Shanghai, China

Purpose: Congenital cataract is an important cause of visual impairment in childhood. Our previous study reported that the c.110G>C (p.R36P) mutation in the γD-crystallin gene (CRYGD) was associated with congenital cataract in a Chinese family. This study aimed to investigate the potential underlying mechanism through which the p.R36P mutation leads to congenital cataract.

Methods: Plasmids encoding wide-type human γD-crystallin and the mutant R36P γD-crystallin were transfected into HEK293T and SRA01/04 cells. Protein expression levels, including total, soluble, and insoluble fractions, were quantified by Western blotting. Quantitative reverse transcription-polymerase chain reaction (RT-PCR) was used to assess the mRNA expression of other crystallin genes. Cell viability and apoptosis were evaluated using the CCK-8 assay and flow cytometry, respectively.

Results: The total protein, especially the soluble fraction, was significantly reduced in the R36P mutant, while the insoluble part remained unaffected. The decrease of soluble R36P γD-crystallin could not be rescued by the proteinase inhibitor MG132. The mRNA expression of the R36P mutation was lower, but other crystallin RNAs were unchanged. Cell viability was slightly decreased (11%, $p<0.05$), and cell apoptosis was not significantly increased (12%, $p=0.31$).

Conclusions: The significant decrease in soluble R36P γD-crystallin may represent a novel mechanism underlying congenital cataract caused by CRYGD gene mutation.

Cataract is the primary cause of blindness globally, which is caused by the opacity of the crystalline lens. The most common type is congenital cataract, which presents at birth or early in the postnatal period and is the main cause of visual impairment in children. About 20,000–40,000 children each year are born with congenital cataract worldwide [1], and over 18% have a positive family history of cataract [2]. Investigation of the genetic etiology and underlying mechanisms of congenital cataract could improve the current understanding of its development and progression.

The bulk of the lens is formed by crystallins, an important structural protein in lens epithelial and fiber cells. There are two families of crystallins in the human lens: alpha-crystallins (α-crystallins) and beta/gamma-crystallins (β/γ-crystallins). The first, α-crystallins, are a type of small heat-shock protein that protect the lens against physiological stress, and they are found in both lens epithelial cells and fiber cells. Meanwhile, β/γ-crystallins are expressed mainly in lens fiber cells, and their main function relates to the structural integrity of the lens. The transparency of the lens depends on both short-range interactions between crystallins [3] and the solubility of these proteins [4]. A growing body of research has shown that crystallin mutations eventually lead to the development of cataract.

Currently, nearly 2,000 variants concerning over 400 genes have been identified in inherited congenital cataract, and 16 crystallin family genes have been identified in these cases (Cat-Map) [5]. For the more widely distributed chaperone α-crystallins, gene mutations could cause cataract, possibly accompanied by myopathy [6]. Knockout of αA- and αB-crystallin genes (CRYAA and CRYAB) in mice has been shown to lead to cataract formation [7]. For the stable structural protein β/γ-crystallins, mutations can result in an abnormal protein structure and the aggregation of unstable proteins in the lens. Mutations in β-crystallins tend to cause various cataract phenotypes, such as cerulean or zonular pulverulent cataract, while mutations in γ-crystallins tend to cause nuclear or zonular cataracts [8].

γ-Crystallins are the major protein constituents in the nucleus of the vertebrate lens. Compared to the well-studied α-crystallins, the functions of β- and γ-crystallins are not yet fully understood. In the human lens, only γC-crystallin and γD-crystallin are highly expressed in considerable concentrations. Previous researchers have identified point mutations,

Correspondence to: Li Wang, Department of Ophthalmology, Eye and ENT hospital of Fudan University, No. 83 Fenyang Road, Shanghai, China; email: Li_wang@fudan.edu.cn

insertions, or deletion mutations in the γD-crystallin gene (CRYGD) in congenital cataract families. For example, the recurrent P24T mutant of γD-crystallin (c.70C>A) was shown to be a hot-point mutation for congenital coralliform cataracts [9,10], and the altered solubility of the P24T mutant causes increased turbidity in the lens in vitro [11]. In our previous study, we confirmed that the c.110G>C mutation in exon 2 of CRYGD was associated with autosomal dominant congenital cataract in a Chinese family [12]. However, the underlining mechanisms remained unknown. In this study, we aim to investigate the expression patterns of the mutants in an attempt to better understand the possible pathogenesis of cataract.

METHODS

Homology modeling and alignment: The amino acid sequence of Human gamma D-crystallin (HGD) protein (NP_ 008822.2) was downloaded from NCBI protein database. The initiator methionine residue is numbered zero. The three-dimension protein structures of HGD and R36P were generated by an online I-TASSER server. The aligned structures of HGD and R36P were further processed and visualized using the PyMOL molecular graphics system (v. 2.4.1; Schrodinger, LLC, San Diego, CA).

Construction of wild-type human γD-crystallin and mutant-type R36P plasmid: Wild-type plasmid with human full-length CRYGD cDNA (NM_006891) was originally constructed using the pcDNA3.1 vector tagged with 3xFlag. Missense mutation (c. 110G>C) was introduced using a KOD plus mutagenesis kit (TOYOBO, Osaka, Japan) with site-directed primer pair (5′-CCG TGG ACA GCG GCT GCT GGA TGC TCT ATG-3′,5′-GCG CCG AGT TGC AGC GGC TCA AGT AG-3′). *E. coli* DH5α competent cells were transformed with these vectors following the manufacturer's instructions (TaKaRa, San Jose, CA). Wild-type CRYGD and mutant-type R36P plasmids were extracted and purified using a Plasmid Mini Kit I (D6943–01, Omega Therapeutics, Albuquerque, NM). The construct sequences were confirmed by direct sequencing.

Transduction of the plasmid: To study the effect of the R36P mutation on HEK293T and human lens epithelial SRA 01/04 cells, Lipofectamine 3000 (Thermo Fisher, Waltham, MA) was used for transfection. HEK293T and SRA 01/04 cells were cultured in DMEM/HighGlucose (Merk, Darmstadt, Germany) supplemented with 10% fetal bovine serum (Gibco, Thermo Fisher) and a 1% penicillin–streptomycin solution (Thermo Fisher). Cells were seeded onto six-well plates at a confluence of 60% before transfection (appendix 1). The master mix containing wild-type or mutant CRYGD constructs was prepared at a concentration of 10 ng/μl, and 250 μl of solution was added per well. Following 6 h of incubation, the culture media was changed. Passages 4–10 of SRA 01/04 and passages 10-30 of HEK293T cells were used in this study.

Western blot (WB) analysis: Cells were harvested 48 h after transfection and lysed on ice using 1% Triton X-100. Then, the soluble and insoluble parts were separated through centrifugation at 12,000 g for 15 min. The insoluble part was further lysed by sonication in radioimmunoprecipitation assay (RIPA) buffer. After protein denaturation, equal amounts of samples were loaded on sodium dodecyl sulfate-polyacrylamide gel for electrophoresis (SDS–PAGE) and transferred to polyvinylidene fluoride membranes. After blocking, the membranes were incubated with antibodies against Flag (1:5000; Proteintech, Rosemont, IL), γD-crystallin (1:1000; GeneTex, CA) and GAPDH (1:3000; Proteintech). After the secondary antibody incubation, the bands were visualized using ECL western blotting substrate (Thermo Fisher) and digitalized using ImageJ (version 1.52a; NIH, MD). To evaluate total protein expression, the proteinase inhibitor MG132 was added 24 h before cell harvest in one set of samples.

Cell viability and apoptosis: Cell viability was evaluated using the Cell Counting Kit-8 (CCK-8) assay. Cells were seeded into 96-well plates before the test. First, 10 μl of CCK-8 solution (Dojindo Molecular Technologies, Rockville, MD) was added, followed by 4-h incubation. Then, the absorbance at 450 nm was measured using a microplate reader (Spark multimode reader; Tecan, Männedorf, Switzerland). Cell viability was calculated based on the following equation: cell viability (%)=($A_{transfected} - A_{blank}$)/ ($A_{control} - A_{blank}$) × 100% (A=absorbance).

Cell apoptosis was detected by flow cytometer (MoFlo XDP, Beckman Coulter, Brea, CA) using Annexin V-FITC apoptosis assay kit (abs50001, Absin, Shanghai, China). The transfected cells were collected by 0.25% trypsin (Gibco, Thermo Fisher Scientific) at 37 °C, washed and resuspended to the density of 1 x 10^6 cells/ml by binding buffer on ice. 5 μl Annexin V-FITC and 5 μl Propidium Iodide were added to 500 μl cell suspension separately, and then cell suspension were incubated at room temperature in the dark for 15 min and 5 min separately. Cell apoptosis data were analyzed by FlowJo software (FlowJo V10, Ashland, OR).

Immunocytochemistry: First, transfected cells were fixed, permeated, and blocked. Then, a monoclonal anti-Flag (1:1000; Proteintech) antibody was used to incubate the cells overnight. After washing, the cells were incubated with CY3-conjugated goat anti-mouse secondary antibody (1:500, Thermo Fisher). DAPI staining was used for nuclear

Table 1. Primer sequences used in amplification.

Genes	Forward primers	Reverse primers
CRYAA	ATCCACGGAAAGCACAACG	ATGCCATCGGCAGACAGG
CRYBA1	CCTACCACATTGAGCGTCTC	CACTGGCGTCCAATAAAG
CRYBB2	TGACGATGTACCCAGCTTCC	TGCTGTCCTTGTAGTCTCCCT
CRYGC	GCAATGGATGGGCCTCAGCGACTCC	GGCAGTCTTCACTCAGCTCCAT
CRYGD	CGGCTGCTGGATGCTCTA	GAACTCTATCATCTGGCCTCTGT
CRYGS	AGAGCTGTTCATCTGCCTAG	CAATCTTCGGTGGTTTCA

visualization, and images were captured by fluorescence microscopy (Leica, Wetzlar, Germany).

Real-time polymerase chain reaction: Total RNA was extracted from cells using an EZ-press RNA purification kit (EZbioscience, Roseville, MN). cDNA was synthesized using a PrimeScript RT reagent Kit (Takara). Then, amplification and quantification were performed using an SYBR Premix Ex Taq kit (Takara) on a 7500 Real-Time PCR System (Applied Biosystems, Thermo Fisher). The primers are listed in Table 1.

Statistical analysis: All experiments were performed using at least three independent samples for data analysis. The exact number of biologic replicates is explained in the corresponding figure legend. Statistical analysis was performed using Statistical Product and Service Solutions (SPSS; version 23, IBM) and plotted into graphs using Prism (version 6, GraphPad). The Kruskal–Wallis test was used to compare protein and relative mRNA concentrations among the three groups with different variances or non-normal distributions. A one-way analysis of variance (ANOVA) with post hoc multiple comparisons was used to compare the cell viability of the three groups. The Student's t test was used to compare differences in protein and relative mRNA concentrations between two groups, which exhibiting equivalent variance and normal distribution. A p-value <0.05 was considered statistically significant.

RESULT

The R36P mutation on the structure of γD-crystallin: The predicted structure of R36P mutation is presented in Figure 1A. The c. 110G>C mutation in exon 2 of CRYGD resulted in the substitution of arginine with proline at residue 36, which was located in the second Greek key motif (the upper panel of Figure 1A). The plasmids encoding of the wide type (human gamma-D crystallin, HGD) and mutant (R36P) forms of γD-crystallin were constructed according to the sequences shown in the lower panel of Figure 1A. The structural diagram of the pcDNA-CRYGD-FLAG plasmid is shown in Figure 1B.

R36P mutation results in lower γD-crystallin expression in HEK293T cells: The expression levels of HGD or R36P γD-crystallin were determined in transfected HEK293T cells. Both groups expressed proteins labeled with the flag tag (Figure 2A). However, the protein expression of R36P was significantly reduced to 52.4% compared to that of wild-type HGD (Figure 2A,B, $p<0.05$, Kruskal-Wallis test, n=3). Concurrently, the cell viability was also reduced by 11.3% in the R36P group ($p<0.01$, one-way ANOVA, n=6; Figure 2C).

Effect of R36P mutation on γD-crystallin in SRA 01/04 cells: We investigated the effect of R36P mutation on SRA 01/04 cells, a transformed human lens epithelial cell line. After transfection for 48 h, the flag-tagged proteins were successfully detected through whole-cell lysis. Similar to the results for HEK293T cells, the expression of the Flag tag and γD-crystallin was reduced to 35.8% and 34.5%, respectively with statistical significance ($p<0.05$, Kruskal-Wallis test, n=3; Figure 3A–C). Additionally, the distribution of the flag-tagged proteins was visualized using immunocytochemistry (Figure 3D). The wild-type HGD was located in the nucleus and the cytoplasm as showed in the upper images, which is the normal physiological distribution.In contrast, the R36P mutant exhibited a preference for locating in the cytoplasm near the cell membrane, and the cells displayed a more slender shape with indistinct boundaries, compare with wild-type cells. Considering the evidence of altered cell viability in HEK293T cells and changes in the morphology of SRA cells, we then investigated the effect of R36P on cell apoptosis. Contrary to our expectation, there was no statistically significant difference in cell apoptosis between the wild-type HGD and the R36P mutant (Appendix 2). According to the protein–protein interaction analysis (String-DB), the functional protein association of γ-crystallin is also related to gap junction PF00029 and tight junction PF00822. However, the selected markers (zo-1, connexin 46, claudin-1, e-cadherin and n-cadherin) of these pathways appeared to be unchanged in R36P-transfected SRA cells (Appendix 3).

The decreased soluble portion of R36P mutants in SRA 01/04 cells: The soluble and insoluble fractions of the protein

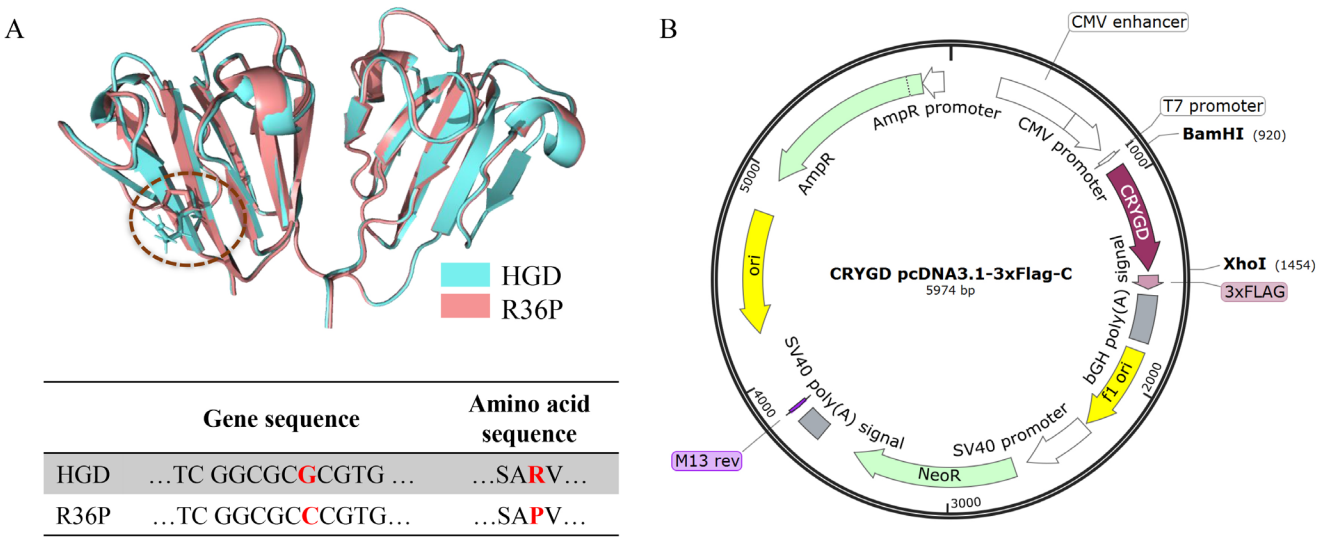

	Gene sequence	Amino acid sequence
HGD	…TC GGCGC**G**CGTG …	…SA**R**V…
R36P	…TC GGCGC**C**CGTG…	…SA**P**V…

Figure 1. The structure of HGD and R36P proteins and plasmids. **A**: The No.36 amino acid side chain is highlighted by a dashed-dotted red line, the corresponding sequences are listed below. **B**: Schematic diagram of HGD plasmid structure.

lysates were separated for detailed quantification. The soluble portion of R36P was significantly reduced to 9.8% of the HGD level (upper panel of Figure 4A), while the insoluble portion was statistically insignificant between the two groups (lower panel of Figure 4A). The calculated intensity ratios of insoluble to soluble parts in the HGD and R36P groups were 0.87±0.21 and 7.60±1.63, respectively ($p<0.01$, Student's *t* test, n=3). The proteasome inhibitor MG132 did not change the reduction in the soluble portion or the identical concentration of the insoluble portion observed with the R36P mutant (Figure 4B).

mRNA expression of other crystallin proteins of lens: Further, we compared the mRNA expression levels of the different crystallin proteins using real-time PCR (Figure 5). The mRNA expression of γD-crystallin increased by 221,000 times after transfection in wild-type HGD group, but the R36P mutants only increased 109,000 folds, lower than that of HGD group with statistical significance ($p<0.01$, Kruskal-Wallis test, n=4). The mRNA expression of αA-, αB-, βB-, γC-, and γS-crystallin genes remained statistically unaffected by the R36P mutant ($p=0.48$, 0.4, 0.28, 0.73 and 0.46 in turn, Student's t-test, n=3-4).

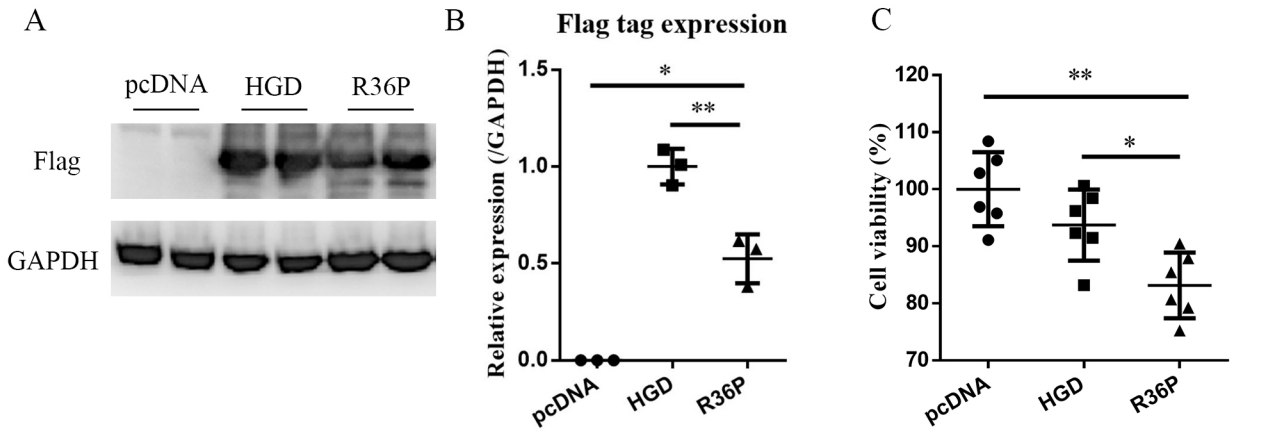

Figure 2. Effect of R36P mutation on protein expression levels and cell viability in HEK293T cells. **A**: SDS–PAGE analysis of protein labeled with flag tag. **B**: Densitometry analysis of the relative protein expression of flag-tagged γD-crystallin (*$p<0.05$, Kruskal–Wallis test, n=3). **C**: Cell viability of the HEK293T cells after transfection for 48 h (**$p<0.01$, one-way ANOVA, n=6).

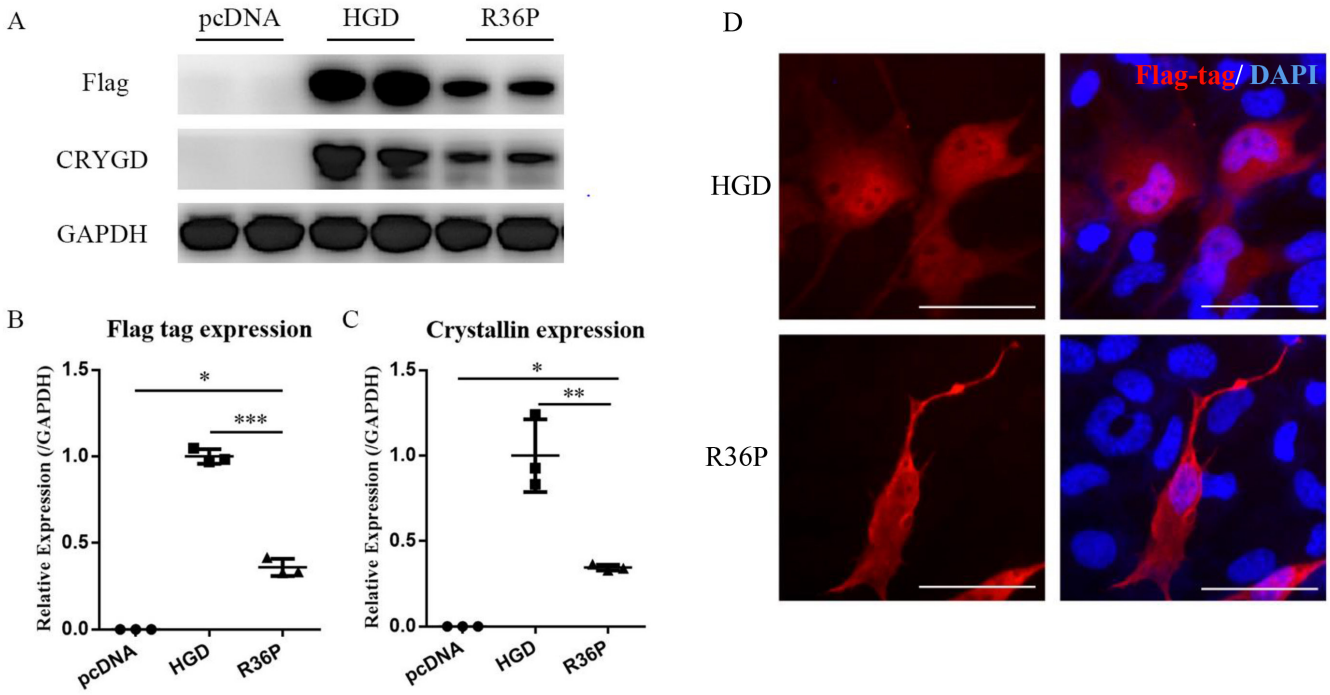

Figure 3. Effect of R36P mutation on SRA 01/04 cells. **A**: Western blot of the whole-cell lysis from transfected SRA 01/04 cells. **B**, **C**: Densitometry analysis of the relative protein expression levels of flag-tagged γD-crystallin (*p<0.05, **p<0.01, ***p<0.001, Kruskal–Wallis test, n=3). **D**: Immunocytochemistry images of transfected SRA cells. The tagged proteins were stained with red fluorescence, and the nuclei were visualized using DAPI (blue). Representative photos of triplicates are shown. Scale bar: 50 µm.

DISCUSSION

The human lens is transparent and inhomogeneous and grows continuously throughout life, with the main function of focusing incoming light onto the retina. The structural proteins in lens, including α- and β/γ-crystallins, are densely packed within cells. Of these, γ-crystallins are found predominantly in the nuclear region of the lens, especially in embryonic nuclear region, where they are found in particularly high concentrations [13]. Numerous publications have reported that various CRYGD mutations are associated with

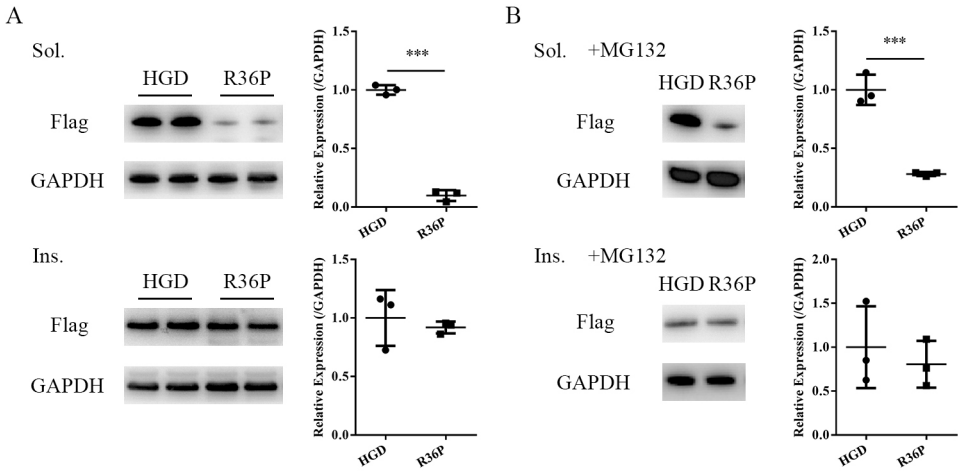

Figure 4. The expression levels of soluble and insoluble flag-tagged proteins in SRA 01/04 cells. **A**: Western blot and semi-quantification of soluble and insoluble flag-tagged proteins. (***p<0.001, Student's *t* test, n=3). **B**: Western blot and semi-quantification of soluble and insoluble flag-tagged proteins after treatment with proteasome inhibitor MG132 (***p<0.001, Student's *t* test, n=3).

nuclear, coralliform, or lamellar cataract formation. In our previous study, we also found bilateral and central nuclear opacity in affected family with congenital cataract. Unlike the higher density of crystalline particles observed within the lens nucleus in cases with the R36S mutation, which is attributed to abnormal crystallization [14], the R36P mutation in the case we studied presented as a central cloudy opacity in the lens. This suggests that the same amino acid site in γD-crystallin may give rise to different cataract phenotypes through distinct causative mechanisms.

In this research, we demonstrated a potentially novel mechanism underlying the effect of the γD-crystallin mutation in congenital cataract. Currently, most cataract-causing mutants in γD-crystallin have been found to result in unstable proteins prone to aggregation. However, we identified a different phenotype associated with R36P mutation. The mRNA and total protein levels of R36P were significantly reduced, even though the absolute amount of precipitated proteins was unaltered. Moreover, the decreased level of R36P proteins could not be restored by inhibition of proteasome degradation, suggesting the reduction was due to decreased protein synthesis.

The reason for such difference is unknown, but it can be speculated that the R36P mutation may effect transcription efficacy through its impact on exonic *cis*-elements and/or nonsense-mediated mRNA decay (NMD). Exonic mutations can induce the splicing machine to skip the mutant exons [15], thereby inactivating the gene through pre-mRNA modification. Additionally, the missense mutation or splicing abnormality may cause mRNA degradation during quality inspection, via the NMD pathway [16]. This mechanism has been observed in several congenital diseases, such as severe dilated cardiomyopathy with LMNA (encoding lamins A and C) missense mutations [17]. However, it has not yet been reported in cataract-causing crystallin gene mutations.

The soluble fraction of γD-crystallin was greatly reduced in the R36P mutant. According to studies on healthy lenses, protein-rich lenses maintain transparency due to the spatial order of the molecules. As the physiological concentration (404 mg/ml), the crystallins exhibit short-range order, similar to a glassy state. However, upon dilution within a limited range, the crystallins gradually transition into independent scatterers, causing the lens to appear turbid [3]. It is presumed that the pronounced decrease in the concentration of soluble γD-crystallin might contribute to the development of nuclear cataract, the predominant site of γD-crystallin distribution. Further, as water-soluble crystallins decrease with aging, this could theoretically accelerate cataract progression.

Notably, the ratio of precipitated to soluble proteins was significantly increased in the R36P mutant, suggesting the insolubility of the mutative protein. The amino acid at position 36 is located in the β-strand of the Greek key motif, with its side chain exposed on the surface of the protein. The substitution of polar arginine with hydrophobic proline likely

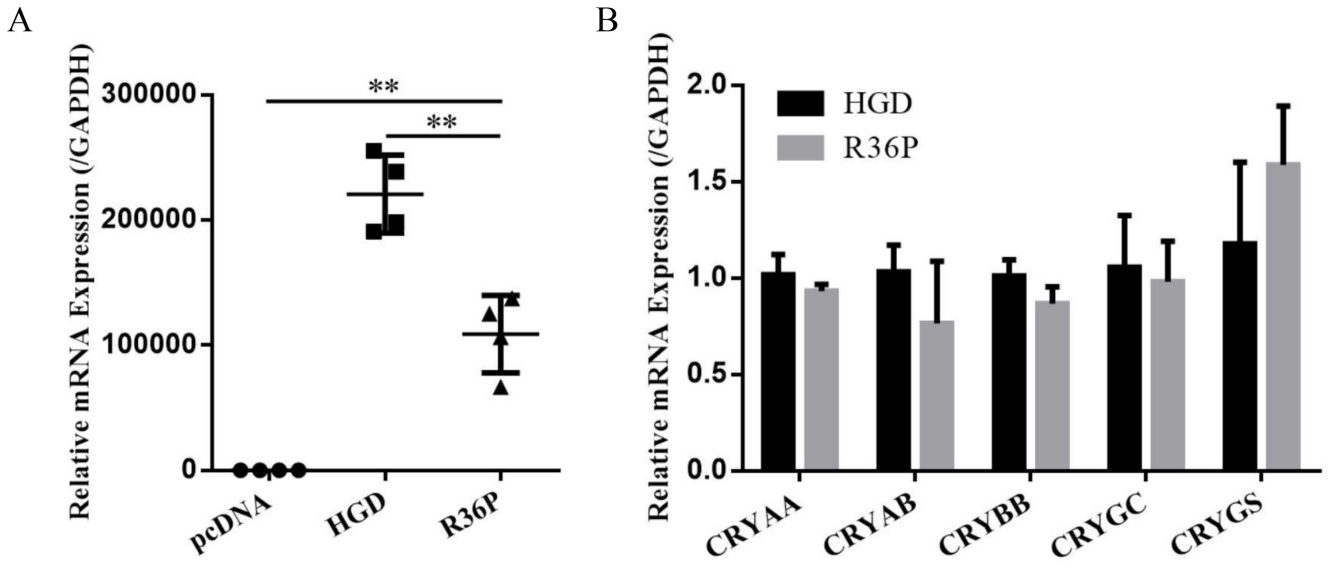

Figure 5. mRNA quantification of different crystallin proteins. **A**: Real-time PCR quantification of CRYGD in transfected SRA 01/04 cells (**p<0.01, Kruskal–Wallis test, n=4). **B**: Quantification of αA-, αB-, βB-, γC-, and γS-crystallin (gene names: CRYAA, CRYAB, CRYBB, CRYGC, and CRYGS) in cells transfected with HGD and R36P (p=0.48, 0.4, 0.28, 0.73 and 0.46 in turn; Student's *t* test, n=3–4).

decreases solubility, which is consistent with the canonical cataract-causing mechanism [18]. In addition, the R36S mutation protein is prone to crystallization, underscoring the importance of the arginine 36 side chain in maintaining solubility. The combination of the aforementioned factors might contribute to nuclear cataract formation.

The subcellular localization of the mutant transformed from a centripetal to a centrifugal distribution. This shift might be the reason for the altered mutant protein synthesis rate and/or trafficking efficiency. The cell shape also changed from a near-cobblestone to a more fibroblast-like oval morphology, suggesting potential cell state transitions. These phenomena have not been observed with other types of crystallin mutation, warranting further in-depth investigation.

Despite the attempt to explore cellular functions, the unchanged nature of the gap and tight junction markers indicates that the R36P expression pattern does not significantly affect cell junctions. In this study, we observed the effects of R36P during a short period due to transient gene expression. Stable transfection models resembling the progressive development of pathology might provide more valuable evidence of cataract formation.

This study has several limitations. Further research is needed to explore the detailed mechanistic changes in mRNA transcription and/or post-transcription processes. In addition, direct investigation of the purified mutant protein and spectroscopic studies are needed.

In conclusion, this study investigated the cataract-causing R36P mutant in human lens epithelial cells for the first time. The expression pattern of CRYGD (c.110G>C) has not been reported in previous congenital cataract studies, potentially expanding the understanding of the mechanisms underlying the development of congenital cataract.

APPENDIX 1. STR ANALYSIS.

To access the data, click or select the words "Appendix 1."

APPENDIX 2. SUPPLEMENTARY FIGURE 1.

To access the data, click or select the words "Appendix 2." Cell apoptosis analysis of HGD and R36P in SRA 01/04 cells. (p=0.31, Student *t* test, n=3).

APPENDIX 3. SUPPLEMENTARY FIGURE 2.

To access the data, click or select the words "Appendix 3." Gap and tight junctions in transfected SRA 01/04 cells. Representative photos of triplicates were shown. (Junction proteins, green; tagged proteins, red; nuclei, blue. Scale bar: 50 μm).

ACKNOWLEDGMENTS

We would like to thank Dr. Xiaolei Lin and Dr. Xin Liu (Eye & ENT Hospital, Fudan University) for kind donation of SRA 01/04 cells. This study was supported by grants from the Shanghai Pujiang Program [18PJD003] and the National Natural Science Foundation of China (No.82171052, 82201172).

REFERENCES

1. Foster A, Gilbert C, Rahi J. Epidemiology of cataract in childhood: a global perspective. J Cataract Refract Surg 1997; 23:Suppl 1601-4. [PMID: 9278811].
2. Wirth MG, Russell-Eggitt IM, Craig JE, Elder JE, Mackey DA. Aetiology of congenital and paediatric cataract in an Australian population. Br J Ophthalmol 2002; 86:782-6. [PMID: 12084750].
3. Delaye M, Tardieu A. Short-range order of crystallin proteins accounts for eye lens transparency. Nature 1983; 302:415-7. [PMID: 6835373].
4. Serebryany E, King JA. The βγ-crystallins: native state stability and pathways to aggregation. Prog Biophys Mol Biol 2014; 115:32-41. [PMID: 24835736].
5. Shiels A, Bennett TM, Hejtmancik JF. Cat-Map: putting cataract on the map. Mol Vis 2010; 16:2007-15. [PMID: 21042563].
6. Fichna JP, Potulska-Chromik A, Miszta P, Redowicz MJ, Kaminska AM, Zekanowski C, Filipek S. A novel dominant D109A *CRYAB* mutation in a family with myofibrillar myopathy affects αB-crystallin structure. BBA Clin 2016; 7:1-7. [PMID: 27904835].
7. Boyle DL, Takemoto L, Brady JP, Wawrousek EF. Morphological characterization of the Alpha A- and Alpha B-crystallin double knockout mouse lens. BMC Ophthalmol 2003; 3:3-[PMID: 12546709].
8. Hejtmancik JF. Congenital cataracts and their molecular genetics. Semin Cell Dev Biol 2008; 19:134-49. [PMID: 18035564].
9. Yang G, Chen Z, Zhang W, Liu Z, Zhao J. Novel mutations in CRYGD are associated with congenital cataracts in Chinese families. Sci Rep 2016; 6:18912-[PMID: 26732753].
10. Cai SP, Lu L, Wang XZ, Wang Y, He F, Fan N, Weng JN, Zhang JH, Liu XY. A mutated *CRYGD* associated with congenital coralliform cataracts in two Chinese pedigrees. Int J Ophthalmol 2021; 14:800-4. [PMID: 34150533].
11. Khan AR, James S, Quinn MK, Altan I, Charbonneau P, McManus JJ. Temperature-Dependent Interactions Explain Normal and Inverted Solubility in a γD-Crystallin Mutant. Biophys J 2019; 117:930-7. [PMID: 31422822].

12. Wang L, Chen X, Lu Y, Wu J, Yang B, Sun X. A novel mutation in γD-crystallin associated with autosomal dominant congenital cataract in a Chinese family. Mol Vis 2011; 17:804-9. [PMID: 21527994].

13. Vendra VP, Khan I, Chandani S, Muniyandi A, Balasubramanian D. Gamma crystallins of the human eye lens. Biochim Biophys Acta 2016; 1860:1 Pt B333-43. [PMID: 26116913].

14. Kmoch S, Brynda J, Asfaw B, Bezouska K, Novák P, Rezácová P, Ondrová L, Filipec M, Sedlácek J, Elleder M. Link between a novel human gammaD-crystallin allele and a unique cataract phenotype explained by protein crystallography. Hum Mol Genet 2000; 9:1779-86. [PMID: 10915766].

15. Cartegni L, Chew SL, Krainer AR. Listening to silence and understanding nonsense: exonic mutations that affect splicing. Nat Rev Genet 2002; 3:285-98. [PMID: 11967553].

16. Brogna S, Wen J. Nonsense-mediated mRNA decay (NMD) mechanisms. Nat Struct Mol Biol 2009; 16:107-13. [PMID: 19190664].

17. Kato K, Ohno S, Sonoda K, Fukuyama M, Makiyama T, Ozawa T, Horie M. *LMNA* Missense Mutation Causes Nonsense-Mediated mRNA Decay and Severe Dilated Cardiomyopathy. Circ Genom Precis Med 2020; 13:435-43. [PMID: 32818388].

18. Li J, Chen X, Yan Y, Yao K. Molecular genetics of congenital cataracts. Exp Eye Res 2020; 191:107872[PMID: 31770519].

Articles are provided courtesy of Emory University and the Zhongshan Ophthalmic Center, Sun Yat-sen University, P.R. China. The print version of this article was created on 26 June 2024. This reflects all typographical corrections and errata to the article through that date. Details of any changes may be found in the online version of the article.